International Journal of Nanoelectronics and Materials
IJNeaM
ISSN 1985-5761 | E-ISSN 2232-1535

The thermal conductivity of van der Waals hexagonal boron nitride/graphene heterostructure: A combined equilibrium molecular dynamics (EMD) and density functional theory (DFT) study

Dharma Darren Ram [a], Muhammad Aniq Shazni Mohammad Haniff [a] *, and Mohd Ambri Mohamed [a]

[a]*Institute of Microengineering and Nanoelectronics, Universiti Kebangsaan Malaysia, 43000, Bangi, Selangor, Malaysia*
∗Corresponding author. e-mail: aniqshazni@ukm.edu.my

Received 21 April 2025, Revised 21 August 2025, Accepted 24 September 2025

ABSTRACT

Two-dimensional van der Waals (vdW) heterostructures are critical for advancing nanoscale thermal management in next-generation electronics. Hexagonal boron nitride (h-BN) and graphene, with their structural similarity and minimal lattice mismatch (1.8%), offer unique advantages as hybrid heat-spreading materials. This study investigates the thermal conductivity of single-layer h-BN/graphene (SLh-BN/SLG) heterostructures using equilibrium molecular dynamics (EMD) simulations based on the Green–Kubo method, evaluating both in-plane and out-of-plane phonon transport. Density functional theory (DFT) calculations elucidate phonon dispersion relations and interfacial interactions, revealing the critical role of low-frequency acoustic phonon modes in governing thermal transport. Results demonstrate that the SLh-BN/SLG heterostructure achieves a thermal conductivity of 1631.9 ± 26.8 $Wm^{-1}K^{-1}$ in the AA stacking configuration—surpassing the AB stacking configurations. This enhancement is attributed to synergistic phonon coupling at the interface, which minimizes scattering losses. The findings highlight the potential of h-BN/graphene heterostructures for efficient heat dissipation in nanoelectronics, providing a foundation for designing devices with precise thermal control.

Keywords: *Graphene, Hexagonal boron nitride, Heterostructure, Thermal conductivity, Equilibrium molecular dynamics, Density functional theory*

1. INTRODUCTION

Thermal conductivity at the interface is one of the important considerations for heat dissipation in the miniaturization of high-power and high-frequency electronic devices, especially at the same length scale as the dominant phonon mean free path. While shrinking the size and increasing the number of transistors on a chip can improve computing capabilities over time, it also contributes to increased power dissipation across devices. Therefore, changes to this device will lead to an inevitable increase in temperature and result in a significant deterioration in the performance and reliability of the device [1]. When the temperature exceeds the normal operating range, where the localized heat released from the device cannot be dissipated efficiently, the device is at risk of overheating and further leads to decreased performance, failure, or explosion. The heat release ability of a material is directly associated with its thermal conductivity. At room temperature, the thermal conductivity of thermal interface materials (TIMs) commonly used in electronic devices is around 0.3 $Wm^{-1}K^{-1}$ for polymer-type materials [2] to 2000 W $m^{-1}K^{-1}$ for single crystal diamond [3]. In addition, the latest TIMs technology involve thermal greases (0.9 to 5 $Wm^{-1}K^{-1}$), phase change materials (0.13 to 0.48 $Wm^{-1}K^{-1}$) [4], and thermal pads (43.3 $Wm^{-1}K^{-1}$) [5]. However, the effectiveness of TIM is still questioned due to the existence of factors such as the thermal degradation of the material, interfacial gaps, and the interfacial roughness [6]. The application of two-dimensional (2D) materials such as graphene, hexagonal boron nitride (h-BN), and transition metal dichalcogenides (TMDs) as heat dissipating materials has shown high potential due to their exceptional thermal, electrical, and electronic properties [7, 8]. The selection of a suitable heat spreader involves the consideration of several important factors such as thermal and electrical conductivity, which determines how much heat can pass across the interface without experiencing any short-circuiting of the device's functionality.

From a physics perspective, 2D materials show different thermal properties compared to their bulk counterparts, including ballistic [9] and hydrodynamic [10] phonon transport properties at temperatures as low as 100 K. Although the in-plane thermal conductivity of 2D materials can be higher, the out-of-plane thermal conductivity is about an order of magnitude lower. For example, the out-of-plane thermal conductivity of graphitic materials are around 6 $Wm^{-1}K^{-1}$, which is significantly lower than its in-plane value of around 2000 $Wm^{-1}K^{-1}$ [3]. Meanwhile, the out-of-plane thermal conductivity of h-BN has been reported as low as 5.2 $Wm^{-1}K^{-1}$ [11], which is lower than the in-plane thermal conductivity value measured in previous studies [12, 13]. This obtained out-of-plane thermal conductivity value can be attributed to non-isotropic phonon scattering in 2D materials consisting of weak van der Waals (vdW) bonds between layers [14]. Another limiting factor for the out-of-plane thermal

conductivity of 2D materials is the phonon interaction with the substrate, which results in a thermal boundary resistance between the 2D material and the substrate. This resistance becomes dominant when the thickness of the 2D material is reduced to length scales equal to the phonon mean free path [15]. Thus, it can limit the ability to dissipate heat vertically across the device.

Phonons are found to be the dominant energy carriers and play an important role for interfacial heat transport in 2D heterostructure materials [16]. It makes a significant contribution to heat transfer when the interface distance is shorter than the phonon wavelength [17]. Several studies on graphene/ h-BN or h-BN/ graphene focus on theoretical approach [18–21], however, the stacking configuration including the AA and AB has not been studied systematically. In the AA arrangement, each atom in the upper layer is directly above the atom in the lower layer [22]. On the other hand, the AB stacking, also known as the Bernal stacking, is common for multilayer 2D materials, that is, some of the atoms in the upper layer are above the central void-space of the hexagon in the lower layer, while the other part is directly above the atoms of the lower layer [23]. To improve heat dissipation and energy efficiency, it is important to understand the concepts and mechanisms of phonon transport across the h-BN/graphene interface. In this study, the thermal conductivity involving phonon transport in the vdW h-BN/graphene heterostructure according to AA and AB stacking configurations was investigated using a combined EMD–DFT. The results of DFT complement these EMD simulations, elucidating how interfacial phonon interactions affect the overall thermal conductivity, where significant changes in the phonon wave vector occur, particularly at the low frequency region. By systematically comparing AA and AB configurations, this study advances the design of 2D heterostructures for efficient nanoscale heat dissipation.

2. METHODOLOGY

2.1. Molecular Dynamics

Initially, the single-layer graphene (SLG) and single-layer hexagonal boron nitride (SLh-BN) models, bilayer graphene (BLG) and bilayer hexagonal boron nitride (BLh-BN) models, and SLh-BN/SLG heterostructure models based on AA and AB stacking configurations are designed with a 100 × 100 Å cell size (4032 atoms per layer and 8064 atoms for the heterostructures) with periodic boundary conditions in the *x*, *y*, and, *z* axes; vacuum padding of ≥20 Å along *z,* as shown in Figure 1(a). The interlayer distance, d_i for BLG, BLh-BN, and SLh-BN/SLG heterostructure was set at 3.4, 3.315, and 3.8 Å respectively, which is comparable with previous experimental works [22, 24]. Classical molecular dynamics (MD) simulations served as the primary tool to assess the thermal conductivity of the models. This approach accounts for atomic interactions and trajectories within a time-evolving simulation framework governed by Newton's second law, where atomic motions are determined by predefined interatomic potentials. In this work, EMD simulations were conducted using the Green-Kubo method. This technique derives thermal conductivity (λ) by integrating the autocorrelation function of the heat flux over the simulation duration, as mathematically represented in Eq. (1) [25, 26]:

$$\lambda = \frac{V}{k_B T^2} \int_{-\infty}^{\infty} \{J(t) \cdot J(0)\}\, dt \qquad (1)$$

where V, k_B, and J denote the system volume, Boltzmann's constant, and the heat flow in the *x*, *y*, and *z* directions, respectively.

The in-plane thermal conductivities (λ_{xy}) of SLG, SLh-BN, and their heterostructures were determined by averaging the *x*- and *y*-directional values under periodic boundary conditions (PBCs). Conversely, the out-of-plane thermal conductivity (λ_z) of the heterostructure was derived from the *z*-directional average. PBCs were implemented across all three spatial dimensions (*x*, *y*, and *z*) to minimize finite-size effects. Achieving convergence in Green-Kubo-based thermal conductivity calculations demands extended simulation durations. To address this, a 1-ns simulation window was adopted, with data from the equilibrated phase

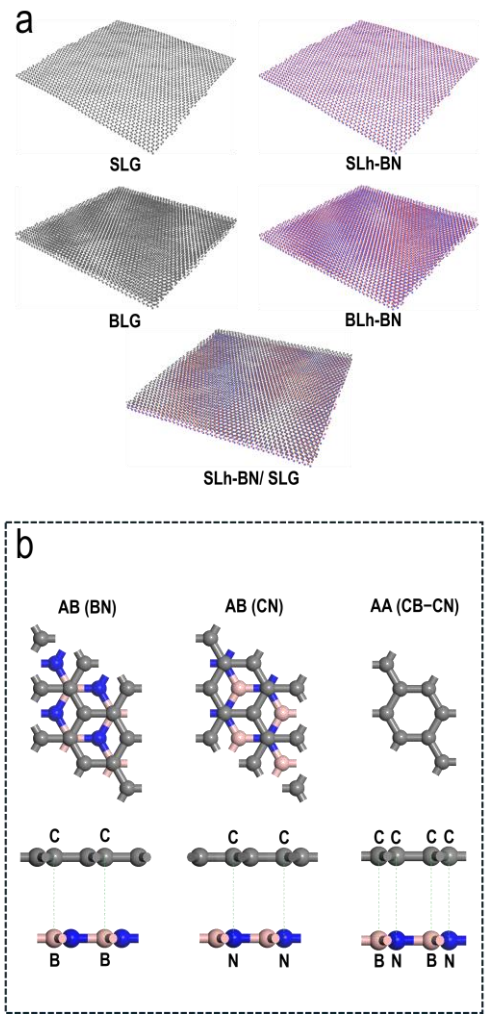

Figure 1. Simulation schematics. (a) Single-layer structure for SLG and SLh-BN models, bilayer structure for BLG and BLh-BN models, and heterostructure for SLh-BN/SLG models (b) Top and side views of SLh-BN/ SLG heterostructure with AB (BN), AB (CN), and AA (CB–CN) configurations used for DFT calculation

(800–1000 ps) used for final λ_{xy} and λ_z computations, as illustrated in Figure 2. The reported λ_{xy} and λ_z represent the arithmetic mean across the five runs, while the associated error bars (± values) correspond to one standard deviation calculated from the set of independent conductivity values for each component. All simulations were executed using the LAMMPS package [27] using 8 cores/16 threads CPU, leveraging its optimized algorithms for heat flux correlation analysis.

The simulations employed the Verlet velocity method to solve the equations of motion, with initial velocities assigned stochastically based on a 300 K thermal seed. Data visualization and analysis were performed using Open Visualizer Tool (OVITO) [28] and Visual Molecular Dynamics (VMD) [29]. For interatomic interactions, the outer layer dynamics were modelled using the Tersoff [30] and AIREBO [31] potentials, whereas interlayer forces were governed by the ILP.BNCH potential [32-34]. To replicate hexagonal boron nitride (h-BN) behaviour, Coulombic interactions between boron and nitrogen atoms were incorporated via the *coul/shield* parameter, applying a shielding cutoff of 16 Å. Periodic boundary conditions were imposed along all (*x, y* and *z*) axes, with the scale of the z-axis being inflated to approximate a suspended layer. Prior to simulation runs, the system underwent two-stage equilibration: first, 1.25 ns in the isothermal-isobaric (NPT) ensemble, followed by 2.5 ns in the canonical (NVT) ensemble, regulated by a Nosé–Hoover thermostat [35]. Thermal conductivity calculations were subsequently conducted in the microcanonical (NVE) ensemble near 300 K.

2.2. Density Functional Theory

First-principles DFT simulations were conducted using the CASTEP code [36]. The generalized gradient approximation (GGA) framework, incorporating the Perdew-Burke-Ernzerhof (PBE) exchange-correlation functional and norm-conserving pseudopotentials, was applied to model SLG, SLh-BN, and their heterostructures. The Grimme method for DFT-D3 correction was selected due to its ability to accurately and efficiently account for vdW force interactions. Structural optimization yielded in-plane lattice parameters of a_{SLG} = 2.4599 Å and $a_{h\text{-}BN}$ = 2.5128 Å, with out-of-plane constants c_{SLG} = 8.3408 Å and $c_{h\text{-}BN}$ = 17.5365 Å, aligning with prior computational benchmarks [37]. In the heterostructure configuration, the h-BN lattice constant ($a_{h\text{-}BN}$ = 2.5128 Å) was adopted, inducing a minor tensile strain (~1.8%) in the SLG component. Computational accuracy was ensured by employing a kinetic energy cutoff of 770 eV and a Monkhorst-Pack k- point grid of 10 × 10 × 4 for Brillouin zone. These parameters were applied to a 2 × 2 × 1 supercell model (Figure 1(b)), with an energy convergence threshold set to 5 × 10^{-7} eV/atom.

3. RESULTS AND DISCUSSION

Our previous phononic studies have shown that the use of h-BN materials and graphene together can increase the thermal conductivity of the entire structure while maintaining the electrical insulation properties of h-BN [21]. Thus, these properties make SLh-BN/SLG heterostructures suitable in nanoscale electronic devices. Table 1 shows the in-plane thermal conductivity (λ_{xy}), out-of-plane thermal conductivity (λ_z), average thermal conductivity (λ_a), and change in distance between layers (Δd) for the single-layer, bilayer and heterostructure models that have been recorded in this study. The average thermal conductivity value obtained for SLG is 2583.2 ± 116.2 $Wm^{-1}K^{-1}$. This value is slightly lower compared to the value obtained experimentally, which is around 2778 ± 569 $Wm^{-1}K^{-1}$ at room temperature [38], which is due to the small size of the simulation domain (100 × 100 Å) and underestimate the contribution of long-wave acoustic phonons. The same behavior has also been found for the average thermal conductivity of SLh-BN, which is around 207.7 ± 9.4 $Wm^{-1}K^{-1}$ compared to the previous study which is over 600 $Wm^{-1}K^{-1}$ [39, 40]. This is due to the use of Tersoff potential parameters that have not been fully optimized, which is the same as the approach taken by previous studies [41].

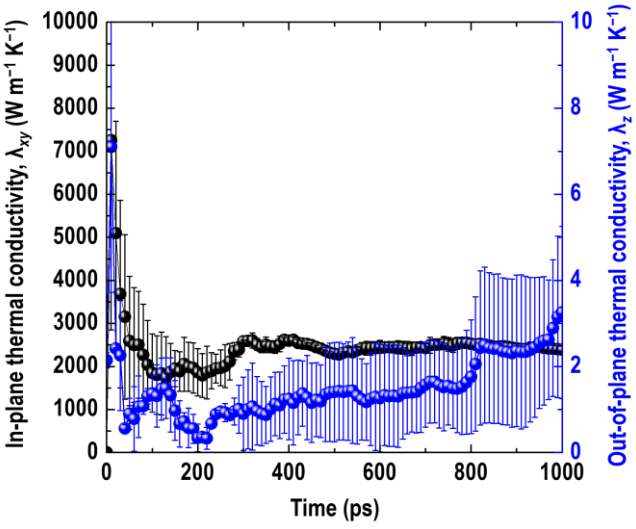

Figure 2. Convergence of in-plane and out-of-plane thermal conductivity of SLh-BN/ SLG model heterostructures with AA (CB–CN) configur ation. This method is repeated for each model

Table 1. The in-plane (λ_{xy}), out-of-plane (λ_{zz}) and average (λ_a) thermal conductivity and changes in interlayer distance (Δd_i) for single-layer structure, bilayer structure and heterostructure in this study

Configuration	In-plane thermal conductivity, λ_{xy} ($Wm^{-1}K^{-1}$)	Out-of-plane thermal conductivity, λ_z ($Wm^{-1}K^{-1}$)	Average thermal conductivity, λ_a ($Wm^{-1}K^{-1}$)	Change in interlayer distance, Δd_i (Å)
SLG	2583.2 ± 116.2	–	2583.2 ± 116.2	–
SLh-BN	207.7 ± 9.4	–	207.7 ± 9.4	–
BLG	175.0 ± 3.0	0.007 ± 0.004	116.7 ± 2.0	0.013–0.022
BLh-BN	139.4 ± 11.6	0.7 ± 0.6	93.2 ± 7.8	0.018–0.046
SLh-BN/ SLG AA (CB-CN)	2461.2 ± 51.9	2.8 ± 0.6	1631.9 ± 26.8	0.091–0.138
SLh-BN/ SLG AB (CB)	1975.8 ± 92.5	2.2 ± 0.1	1317.9 ± 61.6	0.068–0.076
SLh-BN/ SLG AB (CN)	2037.3 ± 127.5	2.5 ± 0.3	1359.1 ± 85.1	0.068–0.072

Meanwhile, the average thermal conductivity obtained for double-layer structures such as BLG and BLh-BN is as expected, with readings of 116.7 ± 2.0 and 93.2 ± 7.8 $Wm^{-1}K^{-1}$ respectively. At room temperature, this bilayer structure was found to have a lower in-plane thermal conductivity value compared to the single-layer structure. These findings indicate that the phonon carriers in the BLG and BLh-BN structures do not act like those in SLG and SLh-BN. This decrease in thermal conductivity can be explained by the suppression of flexural acoustic phonon modes and the appearance of many folding phonon branches that increase Umklapp and normal phonon scattering occurring at the interface [38, 39]. In a bilayer structure, when a phonon crosses the boundary between the two faces, it may experience one or more scattering effects such as specific reflection or diffuse scattering. This phenomenon can cause a loss of coherence in the phonon wave and ultimately impact on the reduction of the overall thermal conductivity. This can be explained by considering phonon scattering using DFT calculations.

Figures 3(a) and (b) show the dependence of phonon energy with phonon wavevector (or momentum) (q) for SLh-BN and AB-BLh-BN. In the single-layer system, six distinct phonon modes are identified: four in-plane modes—transverse acoustic (TA), longitudinal acoustic (LA), transverse optical (TO), and longitudinal optical (LO)—with atomic displacements parallel to the h-BN plane, and two out-of-plane flexural modes (ZA and ZO) involving displacements perpendicular to the plane. For the bilayer AB-BLh-BN structure, the phonon spectrum doubles in complexity due to interlayer coupling, introducing six additional modes. These modes exhibit non-zero frequencies at q = 0 and demonstrate low-frequency shifts attributed to vdW interactions between layers. The enhanced overlap of phonon branches in AB-BLh-BN (dashed blue line) arises from structural factors, including the expanded unit cell dimensions and the altered Brillouin zone geometry associated with bilayer stacking.

In Figures 3(b) and (f), the ZA mode is most significantly affected, where the additional ZA mode at low frequencies corresponds to the out-of-phase vibration [42]. Therefore, phonon energy can transfer from the first layer to the second layer and cause the transmission of low-frequency phonons [43]. For the AB-BLh-BN case, the frequency of the additional mode ZA at the Γ point is about 61.3 cm^{-1} has been obtained in the bilayer structure, which indicates the individual phonon modes are focused. Considering the ZA mode that reaches a maximum frequency of 318.5 cm^{-1} at point K, the frequency of this additional ZA mode includes approximately 19% of the total ZA mode allowed from point Γ to K. For the AB-BLG case as illustrated in Figure 3(d) and (h), the frequency of the additional mode ZA at point Γ (around 169.5 cm^{-1}) is more than twice that of AB-BLh-BN and can reach a maximum frequency of 533.4 cm^{-1} at point K. In general, this is influenced by the average velocity of the ZA mode group and the higher frequency of the ZA mode on graphene compared to h-BN and causes the phonon-phonon interaction to become weaker and further impacts on the increase in heat transport.

For the SLh-BN/SLG heterostructure, the average thermal conductivity values obtained in AA (CB-CN), AB (CB), and AB (CN) configurations are 1631.9 ± 26.8, 1317.9 ± 61.6, and 1359.1 ± 85.1 $Wm^{-1}K^{-1}$, respectively. The average value of thermal conductivity obtained by these three heterostructures is higher compared to the value obtained for BLh-BN and BLG bilayer structures in the AB configuration. When the SLh-BN and SLG layers form a heterostructure, it can be expected that the lattice dynamics of SLh-BN and SLG, especially the ZA mode at low frequencies, are affected by the interfacial layer through vdWs. It is also observed that the SLh-BN/ SLG heterostructure shows a significant phonon dispersion difference compared to BLh-BN and BLG. Figure 4(a–c) shows the phonon dispersion of the AB-BLG structure and the SLh-BN/SLG heterostructure in AA (CB-CN), AB (CB), and AB (CN) configurations. In Figure 4(d–f), a separation between ZA and ZO modes can be observed at the K point for AA (CB-CN), AB (CB), and AB (CN) configurations with values around 65.8, 64.8, and 64.9 cm^{-1}. Meanwhile, the separation between the ZA and ZO modes of AB-BLG is lower which is around 37.5 cm^{-1} (Figure 3(h)). This

significant separation of the SLh-BN/SLG heterostructure is due to the breaking of the equivalence of two carbon atoms in one unit cell and the adsorption of graphene on the h-BN layer [44]. Carbon atoms on top of boron and nitrogen atoms are expected to have stronger vdW interactions compared to carbon atoms on h-BN cavity sites.

A direct method to determine the SLh-BN/ SLG interaction is with the finite energy of the ZA mode at the Γ point (48.3, 62.5, and 64.8 cm^{-1} for AA (CB-CN), AB (CB), and AB (CN) configurations). In the harmonic oscillator model for carbon atomic vibrations, the phonon energy at the ZA mode can be converted into a spring coupling constant, $\alpha_s = 2m\omega^2$, where m is the mass of the carbon atom and ω is the ZA phonon frequency at the Γ point [43]. Through DFT calculations, the values of αs for AA (CB-CN), AB (CB), and AB (CN) configurations are 3.29, 4.26, and 4.42 Nm^{-1}, which increase with the decrease in the change of interlayer distance, Δd (see Table 1). In addition, a decreasing trend in the displacement of the ZO branch can be observed in the Γ → K direction according to the configuration order AB (CN) > AB (CB) > AA (CB-CN), which is a direct effect of the adsorption of carbon atoms on h-BN atoms. Although the interlayer distance change is significant for the AA (CB-CN) configuration, the out-of-plane thermal conductivity is the highest with an average value of 2.8 ± 0.6 $Wm^{-1}K^{-1}$ due to the better phonon coupling between SLh-BN and SLG in the AA configuration compared to the AB configuration, where the carbon atoms are arranged above the boron and nitrogen atoms. This increase in out-of-plane thermal conductivity can be explained by the strength of phonon coupling when the phonon wave vector moves across the interface layer [45].

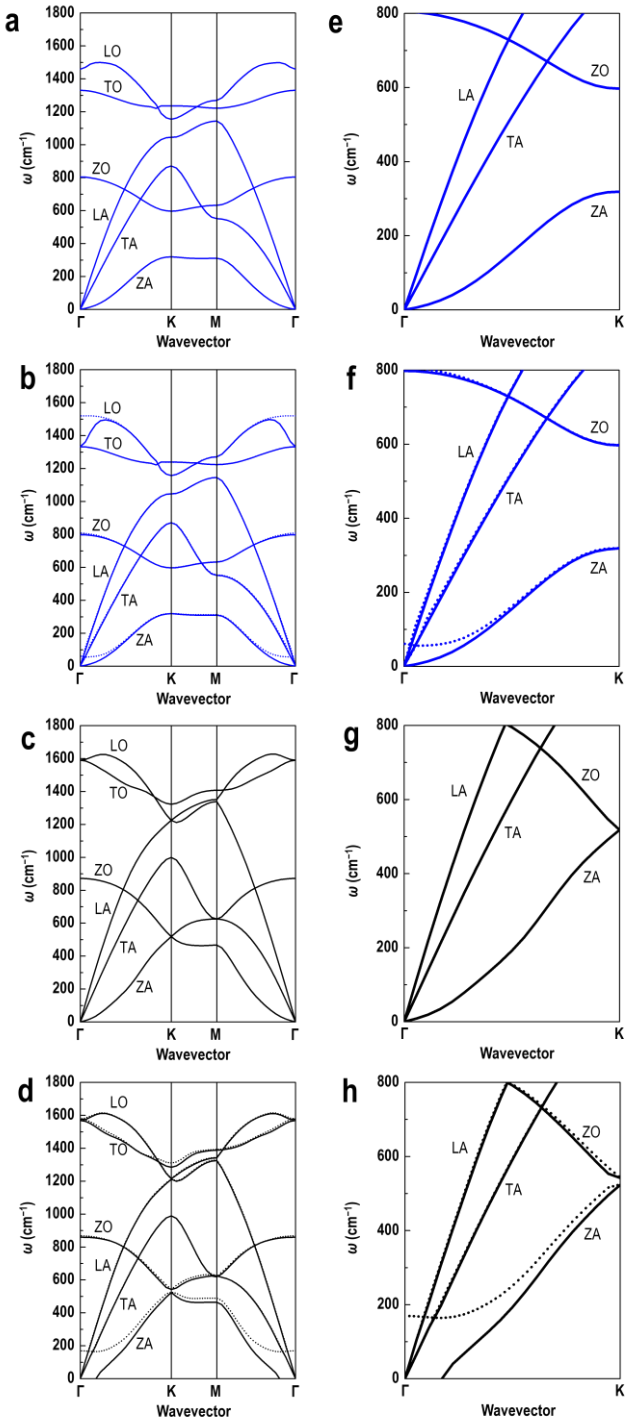

Figure 3. Phonon dispersion for models (a, e) SLh-BN, (b, f) BLh-BN, (c, g) SLG, and (d, h) BLG

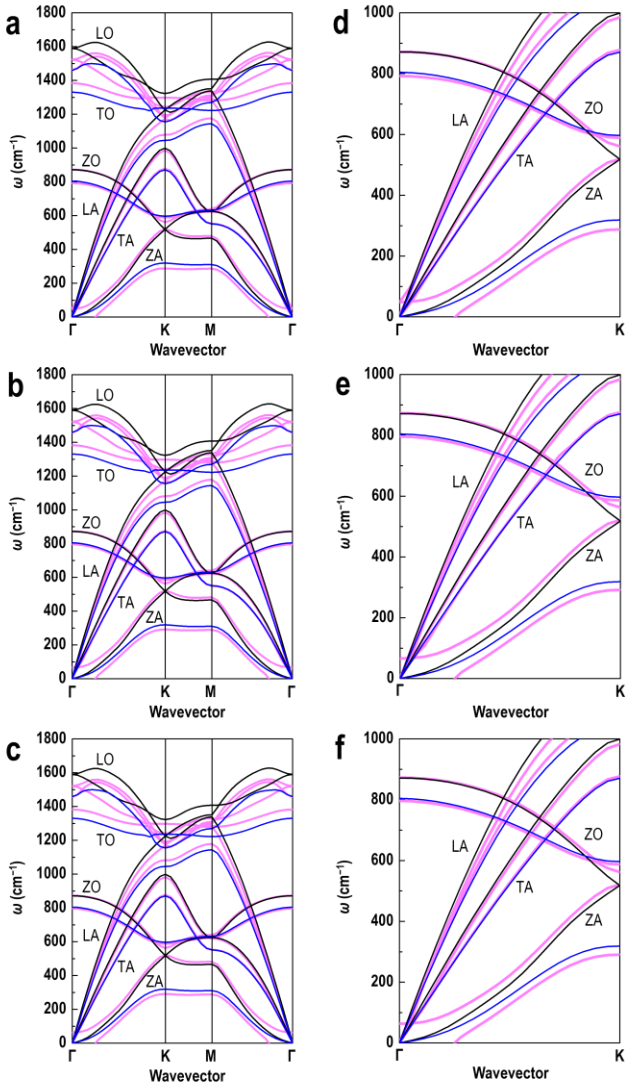

Figure 4. Phonon scattering of the SLh-BN/ SLG heterostructure model according to the configuration (a, d) AA (CB-CN), (b, e) AB (CB), and (c, f) AB (CN). The blue and black lines show the phonon modes of the SLh-BN and SLG models, respectively

4. CONCLUSION

In this study, EMD simulations through the Green−Kubo method were employed to determine the average thermal conductivity of single-layer structures for SLG and SLh-BN models, bilayer structures for BLG and BLh-BN models, and heterostructures for SLh-BN/ SLG models according to AA and AB stacking configuration by considering both λ_{xy} and λ_z values. The phonon distributions for each model were obtained using DFT calculations to explain the phonon interaction at the interface which affects the overall thermal conductivity. The addition of single-layer graphene on top of single-layer h-BN shows a significant increase in thermal conductivity compared to BLG and BLh-BN bilayer structures, thus theoretically supporting the hypothesis. The λ value obtained for the SLh-BN/SLG heterostructure in the AA (CB-CN) configuration is the highest which is 1631.9 ± 26.8 $Wm^{-1}K^{-1}$. The phonon scattering results also observed that the acoustic phonon mode at low frequencies of the SLh-BN/SLG heterostructure plays an important role in determining phonon transport, which is affected by the coupling strength of phonons moving across the interface layer. Compared to the AB (CB) and AB (CN) configurations, the AA (CB-CN) configuration which has a weaker interlayer coupling, i.e. 3.29 Nm^{-1} causes an increased in phonon coupling strength and further contributes to an increase in λ_z values, which is as high as 2.8 ± 0.6 $Wm^{-1}K^{-1}$. Overall, the incorporation of this h-BN layer together with a graphene layer has better potential in the field of nanoscale heat transport and offers useful implications in the development of devices that facilitate effective thermal control and management.

ACKNOWLEDGMENTS

This work was funded by the Ministry of Higher Education (MOHE), Malaysia, under the Fundamental Research Grant Scheme (FRGS/1/2020/STG05/UKM/02/9).

REFERENCES

[1] A. L. Moore and L. Shi, "Emerging challenges and materials for thermal management of electronics," *Materials Today,* vol. 17, no. 4, pp. 163–174, 2014.

[2] D. G. Cahill and R. O. Pohl, "Thermal conductivity of amorphous solids above the plateau," *Physical Review B,* vol. 35, no. 8, pp. 4067–4073, 1987.

[3] L. Wei, P. Kuo, R. Thomas, T. Anthony, and W. Banholzer, "Thermal conductivity of isotopically modified single crystal diamond," *Physical Review Letters,* vol. 70, no. 24, p. 3764, 1993.

[4] B. E. Jebasingh and A. V. Arasu, "A comprehensive review on latent heat and thermal conductivity of nanoparticle dispersed phase change material for low-temperature applications," *Energy Storage Materials,* vol. 24, pp. 52–74, 2020.

[5] Y. Deng and Y. Jiang, "High-performance, safe, and reliable soft-metal thermal pad for thermal management of electronics," *Applied Thermal Engineering,* vol. 199, p. 117555, 2021.

[6] H. Wang, D. W. Ihms, S. D. Brandenburg, and J. R. Salvador, "Thermal conductivity of thermal interface materials evaluated by a transient plane source method," *Journal of Electronic Materials,* vol. 48, pp. 4697–4705, 2019.

[7] H. Song, J. Liu, B. Liu, J. Wu, H.-M. Cheng, and F. Kang, "Two-Dimensional Materials for Thermal Management Applications," *Joule,* vol. 2, no. 3, pp. 442–463, 2018.

[8] F. Duan, D. Wei, A. Chen, X. Zheng, H. Wang, and G. Qin, "Efficient modulation of thermal transport in two-dimensional materials for thermal management in device applications," *Nanoscale,* vol. 15, no. 4, pp. 1459–1483, 2023.

[9] Y. Hu, L. Zeng, A. J. Minnich, M. S. Dresselhaus, and G. Chen, "Spectral mapping of thermal conductivity through nanoscale ballistic transport," *Nature Nanotechnology,* vol. 10, no. 8, pp. 701–706, 2015.

[10] X. Li and S. Lee, "Crossover of ballistic, hydrodynamic, and diffusive phonon transport in suspended graphene," *Physical Review B,* vol. 99, no. 8, p. 085202, 2019.

[11] P. Jiang, X. Qian, and R. Yang, "Time-domain thermoreflectance (TDTR) measurements of anisotropic thermal conductivity using a variable spot size approach," *Review of Scientific Instruments,* vol. 88, no. 7, p. 074901, 2017.

[12] E. Sichel, R. Miller, M. Abrahams, and C. Buiocchi, "Heat capacity and thermal conductivity of hexagonal pyrolytic boron nitride," *Physical Review B,* vol. 13, no. 10, p. 4607, 1976.

[13] H. Zhou *et al.*, "High thermal conductivity of suspended few-layer hexagonal boron nitride sheets," *Nano Research,* vol. 7, pp. 1232–1240, 2014.

[14] X. Gu and R. Yang, "Phonon transport and thermal conductivity in two-dimensional materials," *Annual Review of Heat Transfer,* vol. 19 pp. 1–67, 2016.

[15] Y. Yu, T. Minhaj, L. Huang, Y. Yu, and L. Cao, "In-plane and interfacial thermal conduction of two-dimensional transition-metal dichalcogenides," *Physical Review Applied,* vol. 13, no. 3, p. 034059, 2020.

[16] Y. K. Koh, M.-H. Bae, D. G. Cahill, and E. Pop, "Heat conduction across monolayer and few-layer graphenes," *Nano Letters,* vol. 10, no. 11, pp. 4363–4368, 2010.

[17] V. Chiloyan, J. Garg, K. Esfarjani, and G. Chen, "Transition from near-field thermal radiation to phonon heat conduction at sub-nanometre gaps," *Nature Communications,* vol. 6, no. 1, p. 6755, 2015.

[18] S. Lu and A. J. McGaughey, "Thermal conductance of graphene/hexagonal boron nitride hetero-structures," *Journal of Applied Physics,* vol. 121, no. 11, p. 115103, 2017.

[19] Z.-Y. Ong, G. Zhang, and Y.-W. Zhang, "Controlling the thermal conductance of graphene/h−BN lateral interface with strain and structure engineering," *Physical Review B,* vol. 93, no. 7, p. 075406, 2016.

[20] T. Zhu and E. Ertekin, "Phonon transport on two-dimensional graphene/boron nitride superlattices," *Physical Review B,* vol. 90, no. 19, p. 195209, 2014.

[21] D. D. Ram, M. A. S. M. Haniff, A. M. B. Hashim, and M. A. Mohamed, "Thermal Conductivity of Stacked Hexagonal Boron Nitride (hBN) and Graphene – A

Molecular Dynamics Approach," in *2023 IEEE Regional Symposium on Micro and Nanoelectronics (RSM)*, 2023, pp. 5-8.

[22] A. M. Popov *et al.*, "AA stacking, tribological and electronic properties of double-layer graphene with krypton spacer," *The Journal of Chemical Physics,* vol. 139, no. 15, p. 154705, 2013.

[23] J. D. Bernal, "The structure of graphite," *Proceedings of the Royal Society of London. Series A, Containing Papers of a Mathematical and Physical Character,* vol. 106, no. 740, pp. 749–773, 1924.

[24] O. Hod, "Graphite and Hexagonal Boron-Nitride have the Same Interlayer Distance. Why?," *Journal of Chemical Theory and Computation,* vol. 8, no. 4, pp. 1360–1369, 2012.

[25] M. S. Green, "Markoff random processes and the statistical mechanics of time-dependent phenomena. II. Irreversible processes in fluids," *The Journal of Chemical Physics,* vol. 22, no. 3, pp. 398–413, 1954.

[26] R. Kubo, M. Yokota, and S. Nakajima, "Statistical-mechanical theory of irreversible processes. II. Response to thermal disturbance," *Journal of the Physical Society of Japan,* vol. 12, no. 11, pp. 1203–1211, 1957.

[27] S. Plimpton, "Fast parallel algorithms for short-range molecular dynamics," *The Journal of Chemical Physics,* vol. 117, no. 1, pp. 1–19, 1995.

[28] A. Stukowski, "Visualization and analysis of atomistic simulation data with OVITO–the Open Visualization Tool," *Modelling and Simulation in Materials Science and Engineering,* vol. 18, no. 1, p. 015012, 2009.

[29] W. Humphrey, A. Dalke, and K. Schulten, "VMD: visual molecular dynamics," *Journal of Molecular Graphics,* vol. 14, no. 1, pp. 33–38, 1996.

[30] J. Tersoff, "Empirical interatomic potential for silicon with improved elastic properties," *Physical Review B,* vol. 38, no. 14, p. 9902, 1988.

[31] S. J. Stuart, A. B. Tutein, and J. A. Harrison, "A reactive potential for hydrocarbons with intermolecular interactions," *The Journal of Chemical Physics,* vol. 112, no. 14, pp. 6472–6486, 2000.

[32] I. Leven, T. Maaravi, I. Azuri, L. Kronik, and O. Hod, "Interlayer potential for graphene/h-BN heterostructures," *Journal of Chemical Theory and Computation,* vol. 12, no. 6, pp. 2896–2905, 2016.

[33] I. Leven, I. Azuri, L. Kronik, and O. Hod, "Inter-layer potential for hexagonal boron nitride," *The Journal of Chemical Physics,* vol. 140, no. 10, p. 104106, 2014.

[34] T. Maaravi, I. Leven, I. Azuri, L. Kronik, and O. Hod, "Interlayer potential for homogeneous graphene and hexagonal boron nitride systems: reparametrization for many-body dispersion effects," *The Journal of Physical Chemistry C,* vol. 121, no. 41, pp. 22826–22835, 2017.

[35] S. Nosé, "A molecular dynamics method for simulations in the canonical ensemble," *Molecular Physics,* vol. 52, no. 2, pp. 255–268, 1984.

[36] S. J. Clark *et al.*, "First principles methods using CASTEP," *Zeitschrift für Kristallographie - Crystalline Materials,* vol. 220, no. 5–6, pp. 567–570, 2005.

[37] R. Lynch and H. Drickamer, "Effect of high pressure on the lattice parameters of diamond, graphite, and hexagonal boron nitride," *The Journal of Chemical Physics,* vol. 44, no. 1, pp. 181–184, 1966.

[38] H. Li *et al.*, "Thermal conductivity of twisted bilayer graphene," *Nanoscale,* vol. 6, no. 22, pp. 13402–13408, 2014.

[39] L. Lindsay, D. Broido, and N. Mingo, "Flexural phonons and thermal transport in multilayer graphene and graphite," *Physical Review B,* vol. 83, no. 23, p. 235428, 2011.

[40] L. Lindsay and D. A. Broido, "Enhanced thermal conductivity and isotope effect in single-layer hexagonal boron nitride," *Physical Review B,* vol. 84, no. 15, p. 155421, 2011.

[41] B. Mortazavi and Y. Rémond, "Investigation of tensile response and thermal conductivity of boron-nitride nanosheets using molecular dynamics simulations," *Physica E: Low-dimensional Systems and Nanostructures,* vol. 44, no. 9, pp. 1846–1852, 2012.

[42] B. D. Kong, S. Paul, M. B. Nardelli, and K. W. Kim, "First-principles analysis of lattice thermal conductivity in monolayer and bilayer graphene," *Physical Review B,* vol. 80, no. 3, p. 033406, 2009.

[43] D. Nika, S. Ghosh, E. Pokatilov, and A. Balandin, "Lattice thermal conductivity of graphene flakes: Comparison with bulk graphite," *Applied Physics Letters,* vol. 94, no. 20, p. 203103, 2009.

[44] A. Allard and L. Wirtz, "Graphene on metallic substrates: suppression of the Kohn anomalies in the phonon dispersion," *Nano Letters,* vol. 10, no. 11, pp. 4335–4340, 2010.

[45] H. Rostami, "Theory for shear displacement by light-induced Raman force in bilayer graphene," *Physical Review B,* vol. 106, no. 15, p. 155405, 2022.